



Transition to turbulence in viscoelastic channel flow of dilute polymer solutions

Alexia Martinez Ibarra¹ and Jae Sung Park¹,†

¹Department of Mechanical and Materials Engineering, University of Nebraska-Lincoln, Lincoln, NE 68588-0526, USA

(Received 29 May 2023; revised 28 September 2023; accepted 29 October 2023)

The transition to turbulence in a plane Poiseuille flow of dilute polymer solutions is studied by direct numerical simulations of a finitely extensible nonlinear elastic fluid with the Peterlin closure. The range of Reynolds number (Re) $2000 \le Re \le 5000$ is studied but with the same level of elasticity in viscoelastic flows. The evolution of a finite-amplitude perturbation and its effects on the transition dynamics are investigated. A viscoelastic flow begins transition at an earlier time than its Newtonian counterparts, but the transition time appears to be insensitive to polymer concentration in the dilute and semi-dilute regimes studied. Increasing polymer concentration, however, decreases the maximum attainable energy growth during the transition process. The critical or minimum perturbation amplitude required to trigger transition is computed. Interestingly, both Newtonian and viscoelastic flows follow almost the same power-law scaling of Re^{γ} with the critical exponent $\gamma \approx -1.25$, which is in close agreement with previous studies. However, a shift downward is observed for viscoelastic flow, suggesting that smaller perturbation amplitudes are required for the transition. A mechanism of the early transition is investigated by the evolution of wall-normal and spanwise velocity fluctuations and flow structure. The early growth of these fluctuations and the formation of quasi-streamwise vortices around low-speed streaks are promoted by polymers, hence causing an early transition. These vortical structures are found to support the critical exponent $\gamma \approx -1.25$. Once the transition process is completed, polymers play a role in dampening the wall-normal and spanwise velocity fluctuations and vortices to attain a drag-reduced state in viscoelastic turbulent flows.

Key words: transition to turbulence, non-Newtonian flows

† Email address for correspondence: jaesung.park@unl.edu

1. Introduction

Transition to turbulence has been studied extensively in wall-bounded shear flows for Newtonian fluids since the pioneering work of Reynolds (1883a,b). However, despite many experimental and theoretical contributions (Eckhardt et al. 2007; Schmid 2007; Mullin 2011; Avila, Barkley & Hof 2023), its nature remains unclear even for simple geometries. Reynolds (1883a,b) noted in his experimental pipe flow studies that a strong perturbation can trigger transition at a Reynolds number (Re) of 2260. Subsequent studies have placed this critical Reynolds number in the range of $1760 \le Re \le 2300$ (Kerswell 2005). Through more controlled conditions, it was also shown that the laminar state could be maintained until a higher Reynolds number of Re = 12,000 (extended to 10^5 by Pfenniger 1961). The upper critical Re is in closer agreement with theoretical studies, showing that plane Couette flows (PCF) and pipe flows are linearly stable to infinitesimal perturbations for all Reynolds numbers (Drazin & Reid 1981). For plane Poiseuille flows (PPF), experiments have shown a lower critical Reynolds number of $Re \approx 1000$ (Davies & White 1928; Orszag & Kells 1980; Carlson, Widnall & Peeters 1982), whereas linear stability theory has found that PPF becomes unstable at $Re \approx 5772$ (Orszag 1971). Experimental observations naturally point out the susceptibility of the flow to disturbances in the environment and explain why in practice most pipe and channel flows become turbulent at subcritical Re. In theory, this is further supported by analysis performed on the non-normality of the linearized Navier-Stokes equations, where the efficient amplification of finite-amplitude disturbances at a short time has been identified (Boberg & Brosa 1988; Trefethen et al. 1993; Schmid & Henningson 2001). In contrast to Newtonian flows, the onset of turbulence for non-Newtonian flows or viscoelastic flows of polymer solutions has been relatively less studied. In the remainder of this section, we provide a summary of the relevant literature concerning both Newtonian and viscoelastic flows and present the contributions addressed in the present study.

1.1. Finite-amplitude thresholds in Newtonian flows

Given the strong sensitivity of Newtonian flows to external disturbances, controlled perturbations have been widely utilized in the study of transitional flows. Of particular interest are the disturbances that cause the maximum energy growth in a specified time interval, known as linear optimal perturbations (Farrell 1988; Butler & Farrell 1992). For laminar pipe flow, the linear optimal disturbance is that of a counter-rotating streamwise vortex pair, which evolves into streamwise streaks due to the lift-up mechanism (Landahl 1980; Schmid & Henningson 1994). These optimal perturbations are in agreement with the coherent structures that characterize transitional and turbulent shear flows. However, the transition is often triggered by other structures. Reddy *et al.* (1998) and Peixinho & Mullin (2007) showed that oblique disturbances are more successful at triggering turbulence. Hence, nonlinear optimization approaches have been proposed to compute optimal perturbations (Monokrousos *et al.* 2011; Luchini & Bottaro 2014; Kerswell 2018), proving the existence and efficiency of nonlinear optimal perturbations over the linear ones (Pringle & Kerswell 2010; Cherubini & Palma 2013; Farano *et al.* 2015).

Of greater relevance to the current study is the study of the minimal perturbation amplitude ϵ required to trigger transition. The scaling law describing the relationship between ϵ and Re is also of relevance. Early experimental work used continuous perturbations via a continuous injection of fluid through slits or holes (Rotta 1956; Wygnanski & Champagne 1973). Impulsive perturbations, such as a single-pulse injection of fluid, were also used, showing that these perturbations produced more consistent results by initiating controlled turbulent structures that could be used to determine

turbulence far downstream (Wygnanski, Sokolov & Friedman 1975; Rubin, Wygnanski & Haritonidis 1979; Darbyshire & Mullin 1995). Darbyshire & Mullin (1995) introduced various single-pulse disturbance configurations into a fully developed pipe flow. The critical perturbation amplitude decreased very rapidly with increasing Reynolds number, eventually following an asymptotic behaviour for high Re, regardless of the perturbation type. Hence, this behaviour can be described as $\epsilon = O(Re^{\gamma})$ with the critical exponent $\gamma < 0$, where a large $|\gamma|$ value corresponds to a rapid growth of the disturbances due to nonlinear effects (Trefethen et al. 1993). The current estimate for the critical exponent γ is in the range of $-7/4 < \gamma < -1$ derived from numerical and experimental studies for different geometries. For PPF, Lundbladh, Henningson & Reddy (1994) and Reddy et al. (1998) performed numerical experiments and suggested $\gamma = -7/4$ for both streamwise and oblique perturbations. Chapman (2002) used a formal asymptotic analysis of the Navier-Stokes equations and found $\gamma = -3/2$ and $\gamma = -5/4$ for oblique and streamwise initial perturbations. Experimentally, Philip, Svizher & Cohen (2007) achieved an agreeable scaling factor of $\gamma = -3/2$ for PPF with a shorter channel length. For PCF, Dauchot & Daviaud (1995) experimentally suggested the power exponent of $\gamma = -1$. Instead of using the perturbation amplitude, the kinetic energy of the perturbation E_c has also been examined to suggest a similar scaling law for PCF, where $E_c = O(Re^{\gamma})$, with $-2 \le \gamma \le -2.7$ (Kreiss, Lundbladh & Henningson 1994; Duguet et al. 2013). For pipe flow, Meseguer (2003) numerically studied the formation and breakdown process of streaks due to streamwise vortices, suggesting a critical exponent of $\gamma = -3/2$, in agreement with the formal asymptotic analysis performed by Chapman (2002) for PPF. Through novel experimental set-ups, Hof, Juel & Mullin (2003) and Lemoult, Aider & Wesfreid (2012) uncovered a scaling factor of $\gamma = -1$ for Re > 2000, as proposed by Waleffe & Wang (2005). Lemoult et al. (2012) also showed an exponent close to $\gamma = -3/2$ for the restricted range of 1000 < Re < 2000. Interestingly, Mullin & Peixinho (2006) and Peixinho & Mullin (2006) showed that for Re < 1760 turbulent flows cannot be sustained and all disturbances will eventually decay as $t \to \infty$.

1.2. Transitional behaviour of drag-reducing flows

Since the discovery of Toms (1948), the addition of small amounts of flexible long-chain polymers into a turbulent flow has been known to cause significant drag reduction (DR) in pipe and channel flows. This discovery attracted the interest of several applications that benefited directly from its drag-reducing effects. The most popular application of this phenomenon is in the fossil fuel industry (e.g. Alaska pipeline and fracking fluid). More recently, polymer additives were utilized in a large-scale open-channel watercourse, which showed beneficial reduction in the water depth downstream from the polymer injection point and an increase in the discharge capacity of the channel (Bouchenafa *et al.* 2021).

For viscoelastic effects, one of the most relevant non-dimensional numbers that characterizes polymer solutions is the Weissenberg number (Wi), which is the product of the longest relaxation time of the polymer solution and the characteristic shear rate of the flow. The other most relevant parameter is the elasticity number (El = Wi/Re), which is independent of the velocity, meaning that it is constant for a particular fluid and flow geometry. Hence, the DR phenomenon of polymer solutions in shear flows is typically described in terms of Wi or El (Graham 2014).

The study of viscoelastic fluids has focused mainly on the drag-reducing phenomenon in a turbulent flow (Min *et al.* 2003; White & Mungal 2008; Graham 2014; Xi 2019), whereas the role of polymers on the onset of transition has been relatively less studied. Earlier pipe experiments reported a lower transitional Reynolds number than one required

for Newtonian transition, referred to as early turbulence (Ram & Tamir 1964; Forame, Hansen & Little 1972; Hansen, Little & Forame 1973; Zakin et al. 1977; Draad, Kuiken & Nieuwstadt 1998). Recent experiments showed further possibilities of early transition in pipes and channels at sufficiently high polymer concentrations (Samanta et al. 2013; Srinivas & Kumaran 2017), pointing to the influence of strong elastic effects on the onset of turbulence of polymer solutions. This turbulent state, that results from early turbulence at high polymer concentrations, is referred to as elasto-inertial turbulence (EIT) (Dubief, Terrapon & Soria 2013; Samanta et al. 2013; Terrapon, Dubief & Soria 2015; Sid, Terrapon & Dubief 2018). Chandra, Shankar & Das (2018) expanded the work of Samanta et al. (2013) for higher values of the elasticity number and with various polymer types. For high polymer concentrations, they also found that transition occurred at Re < 2000. This is in agreement with recent results of the linear stability theory of pipe flows by Garg et al. (2018) and Chaudhary et al. (2021), who showed that pipe flows of an Oldroyd-B fluid are linearly unstable. However, it should be noted that Chandra et al. (2018) also observed the delayed transition, in other words, the transitional Reynolds number is increased. The study of EIT has also provided an alternative explanation to the upper limit of turbulent DR, also known as the maximum drag reduction state (Samanta et al. 2013; Choueiri, Lopez & Hof 2018; Lopez, Choueiri & Hof 2019). Interestingly, there are recent studies that have found the nonlinear elasto-inertial exact coherent structures in the EIT regime, named arrowhead structures (Page, Dubief & Kerswell 2020; Buza et al. 2022; Dubief et al. 2022), which link the EIT and elasto-inertial linear instability. An extensive review of these instabilities can be found on Castillo-Sánchez et al. (2022) and Datta et al. (2022).

Similar to subcritical transition in Newtonian flows, a finite-amplitude perturbation is required to trigger the transition of polymer solutions. Hoda, Jovanović & Kumar (2008) studied the energy amplification of perturbations in the form of spatio-temporal body forces in PPF for an Oldroyd-B fluid. They found streamwise-elongated disturbances to be the most amplified. Zhang et al. (2013) expanded this study to a finitely extensible nonlinear elastic fluid with the Peterlin closure (FENE-P) for inertia-dominated PPF. They observed the modal and non-modal types of perturbations, showing either stabilization or destabilization effects of polymer solutions depending on the polymer relaxation time. Agarwal, Brandt & Zaki (2014, 2015) complemented these findings by spanning the bypass transition process for a FENE-P fluid in PPF. They observed the linear and nonlinear growth of an initially located disturbance and found a weakening of the disturbance amplification by polymers. A delay in the onset of transition and a prolonged transition period were also reported. For the natural or orderly transition of polymer solutions, Lee & Zaki (2017) applied an infinitesimally small Tollmien-Schlichting wave to a FENE-P fluid in PPF. They found that the transition scenarios are affected by the level of the elasticity, where a destabilizing effect is observed at the lowest elasticity and a stabilization effect manifests as the elasticity is further increased. Biancofiore, Brandt & Zaki (2017) and Sun, Wan & Zhang (2021) investigated the nonlinear evolution of disturbed streaky structures in viscoelastic Couette and pipe flows, respectively, where viscoelasticity is found to delay the transition to turbulence in time for high Wi.

A power-law scaling of the critical perturbation amplitude, which is analogous to the Newtonian flow that relates ϵ and Re, has not been well explored for polymer solutions even at dilute concentrations and will be studied here. The transition of viscoelastic flows of a dilute FENP-P fluid is triggered by a finite-amplitude perturbation, and the effects of polymers on the transition dynamics and mechanisms are reported. The problem formulation is reported in § 2. The simulation results are presented in § 3. We then conclude in § 4.

2. Problem formulation

We consider an incompressible fluid flow in the plane Poiseuille (channel) geometry driven by a constant mass flux. The x, y and z coordinates correspond to the streamwise, wall-normal and spanwise directions, respectively. Periodic boundary conditions are imposed in the streamwise and spanwise directions with fundamental periods L_x and L_z , respectively. No-slip boundary conditions are applied at the solid walls at $y=\pm h$, where h is the half-channel height. Using the half-channel height h and the Newtonian laminar centreline velocity U_{cl} at the given mass flux as the characteristic length and velocity, respectively, the time t is non-dimensionalized with h/U_{cl} and pressure p with ρU_{cl}^2 , where ρ is the density of the fluid. Utilizing these characteristic scales, the non-dimensional momentum and continuity equations for a fluid velocity u are

$$\frac{\partial \mathbf{u}}{\partial t} + \mathbf{u} \cdot \nabla \mathbf{u} = -\nabla p + \frac{\beta}{Re} \nabla^2 \mathbf{u} + \frac{(1-\beta)}{Re} \nabla \cdot \boldsymbol{\tau}_p, \tag{2.1}$$

$$\nabla \cdot \boldsymbol{u} = 0. \tag{2.2}$$

Here, the Reynolds number for the given laminar centreline velocity is defined as $Re = \rho U_{cl}h/(\eta_s + \eta_p)$, where $(\eta_s + \eta_p)$ is the total zero-shear-rate viscosity. The subscripts 's' and 'p' represent the solvent and polymer contributions to the viscosity, respectively. The viscosity ratio $\beta = \eta_s/(\eta_s + \eta_p)$ (for a Newtonian fluid, $\beta = 1$). For dilute polymer solutions, $(1 - \beta)$ is proportional to polymer concentration; hereinafter, the polymer concentration is represented as $c = 1 - \beta$. The concentration is assumed constant in time and homogeneous in space. Although the viscosity of polymer solutions displays shear thinning, the total shear viscosity is hardly affected by the presence of the polymers for dilute solutions of polymers make a small contribution to the shear viscosity in the first place (Graham 2014). The polymer stress tensor τ_p is modelled by the FENE-P constitutive relation (Bird *et al.* 1987) as

$$\tau_p = \frac{1}{Wi} \left[\frac{\alpha}{1 - \text{tr}(\alpha)/b} - I \right], \tag{2.3}$$

where the Weissenberg number is defined as $Wi = \lambda U_{cl}/h$, where λ is the polymer relaxation time. The parameter b defines the maximum extensibility of the polymers (i.e. $\max{(\text{tr}(\alpha))} \leq b$), which is proportional to the number of monomer units. The polymer conformation tensor $\alpha = \langle qq \rangle$ quantifies the second moment of the probability distribution for the polymer end-to-end vector q, satisfying the evolution equation

$$\frac{\partial \alpha}{\partial t} + u \cdot \nabla \alpha - \alpha \cdot \nabla u - (\alpha \cdot \nabla u)^{\mathrm{T}} = -\tau_p, \tag{2.4}$$

which includes the upper convective derivative of α and stress relaxation due to the elastic nature of the polymer.

Simulations are performed using the open-source code Channelflow written and maintained by Gibson (2012) from which a modified version was made and verified for viscoelastic flows used in the current study (Xi & Graham 2010; Rogge & Park 2022). This study focuses on results for the range of $2000 \le Re \le 5000$. This Reynolds number range for Newtonian flows is found to be subcritical and below the linear stability limit for two-dimensional flows but slightly beyond the transition for three-dimensional flows (Schmid & Henningson 2001). For the viscoelastic cases, the polymer concentration ranges from dilute to semi-dilute regimes: $0.01 \le c \le 0.09$. The Weissenberg number is in the range $32 \le Wi \le 65$. Note that the current study holds the elasticity number constant

at $El \approx 0.017$. The parameter b=5000, which corresponds to a moderately flexible, high-molecular-weight polymer (Xi & Graham 2010, 2012). The extensibility parameter Ex is defined as the polymer contribution to the steady-state stress in uniaxial extensional flow. For the FENE-P model, $Ex=2b(1-\beta)/3\beta$. Significant effects of polymers on turbulence are only expected when $Ex\gg 1$ for a dilute solution $(1-\beta\ll 1)$, which is the case of this study. For the sets of β and b studied, the values of Ex are in the range of 34–330, which is sufficient to observe the effects of polymer solutions (Xi & Graham 2010). This parameter space for the viscoelastic flow is found to be linearly stable (Castillo-Sánchez et al. 2022; Datta et al. 2022).

The equation system above is coupled and integrated in time with a third-order semi-implicit backward differentiation and Adams-Bashforth method for the linear and nonlinear terms, respectively (Peyret 2002). As an effective approach to identifying the self-sustaining process in both Newtonian and viscoelastic flows (Jimenez & Moin 1991; Webber, Handler & Sirovich 1997), the so-called minimal flow unit (MFU) is employed. We use a domain of $L_x \times L_y \times L_z = 2\pi \times 2 \times \pi$ and $4\pi \times 2 \times 2\pi$ to simulate Newtonian and viscoelastic flows, respectively. It is worth noting that viscoelastic MFUs are larger than Newtonian ones to attain sustained turbulence (Wang et al. 2014). A numerical grid system is generated on (N_x, N_y, N_z) (in x, y and z) meshes, where a Fourier-Chebyshev-Fourier spectral spatial discretization is applied to all variables and nonlinear terms are calculated with the collocation method, for which the standard 2/3' dealiasing is used. The numerical grid systems used are $(N_x, N_y, N_z) = (64, 81, 76)$ for the Newtonian simulations and $(N_x, N_y, N_z) = (126, 81, 126)$ for the viscoelastic simulations, unless specified otherwise. The numerical grid spacings in the streamwise and spanwise directions are uniform with $\Delta x^+ \approx 12$ and $\Delta z^+ \approx 7$, respectively, for all cases. In the wall-normal direction, the non-uniform Chebyshev spacing is $\Delta y_{min}^+ \lesssim 0.1$ at the wall and $\Delta y_{max}^+ \approx 5$ at the channel centre.

An artificial diffusivity term $1/(ScRe)\nabla^2\alpha$, with the Schmidt number Sc = 0.5, is added to the right-hand side of (2.4) to improve its numerical stability, as is common practice for spectral simulations of viscoelastic flows (Sureshkumar, Beris & Handler 1997; Dimitropoulos, Sureshkumar & Beris 1998; Xi & Graham 2010, 2012; Rogge & Park 2022). For the range of Re given above, an artificial diffusivity 1/(ScRe) is of the order of 10^{-3} – 10^{-4} , which is much lower than often used in other studies with $1/(ScRe) = O(10^{-2})$ (Sureshkumar et al. 1997; Ptasinski et al. 2003; Li, Sureshkumar & Khomami 2006, 2015). In the low-to-moderate Wi and dilute-to-semi-dilute regimes of the present study, these very small magnitudes of artificial diffusivity should not have a significant impact on the numerical solutions, while still contributing to numerical stability, which has also been confirmed by previous studies (Sureshkumar et al. 1997; Housiadas, Beris & Handler 2005; Li et al. 2006; Kim et al. 2007; Zhu & Xi 2020). Since introducing such an artificial term, an additional treatment for a boundary condition on (2.4) is needed. We update α at the walls using the solution without the artificial diffusivity. These results are then used as the boundary condition to solve (2.4) with the artificial diffusivity term and we then update α for the rest of the channel. The numerical details used in the present study can be found in Xi (2009). The numerical code used here has been extensively validated in the previous studies (Xi & Graham 2010, 2012; Wang et al. 2014; Wang, Shekar & Graham 2017; Rogge & Park 2022).

The initial velocity field is a superposition of the parabolic laminar base flow u_{lam} and a three-dimensional perturbation flow: $u = u_{lam} + au_p$, where a is the magnitude of the perturbation flow field, which is adjustable in the current study. Different laminar base flows u_{lam} are used for Newtonian and viscoelastic flows. The Newtonian laminar flow

is a typical parabolic velocity profile of a plane Poiseuille flow (White 2006), while a viscoelastic laminar flow is obtained from the plane Poiseuille flow solution of a FENE-P fluid (Cruz, Pinho & Oliveira 2005). The viscoelastic laminar flow is a modified version of the Newtonian laminar flow to which contributions due to polymers (i.e. Wi, β and b) are added. In addition, the laminar base state for the polymer stress tensor is also considered (Lee & Zaki 2017). The perturbation field u_p is generated using the subroutine randomfield through Channelflow (Gibson 2012), where its spectral coefficients of the three velocity components are set to decay exponentially with respect to the wavenumber to ensure the smoothness of the flow, similar to turbulent fields. The perturbation field also satisfies no-slip and divergence-free conditions (see Appendix C in Pershin et al. (2022) for details of the subroutine randomfield). This perturbation field is similar to that commonly used for the optimal disturbance to control a transition to turbulence (Farano et al. 2015; Pershin et al. 2022). However, it should be emphasized that the particular form of u_p does not matter as long as it leads to an instability that triggers a transition to turbulence (Faisst & Eckhardt 2004). Owing to the extensional flow nature of transitional and turbulent flows, there are always positive Lyapunov exponents in Newtonian channel flows (Keefe, Moin & Kim 1992; Nikitin 2018) and even viscoelastic channel flows (Stone & Graham 2003), resulting in a quick memory loss of the initial conditions. Darbyshire & Mullin (1995) also experimentally confirmed that different kinds of perturbations result in a very similar stability curve. Nonetheless, the choices of the different forms of the perturbation field were tested, showing similar behaviours such as scaling laws (Mullin 2011). In addition, for optimal perturbations, where the maximum energy growth is efficiently reached during the transition process, similar scaling behaviour was observed (Farano et al. 2015). Therefore, it can be safely assumed that the effect of the perturbation field on the transition to turbulence can be focused only on its magnitude.

Throughout the paper, the perturbation amplitude A is defined as the ratio of the L_2 -norm of the perturbation velocity field u_p to that of the base laminar velocity field u_{lam}

$$A = \frac{\|u_p\|_2}{\|u_{lam}\|_2} = a \sqrt{\int_V u_p^2 \, dV / \int_V u_{lam}^2 \, dV}, \qquad (2.5)$$

where $V = 2L_xL_z$ is the volume of the computational domain. The amplitude squared A^2 can also be referred to the ratio of the kinetic energy of u_p to that of u_{lam} . The perturbation amplitude studied is in the range of $0.014 \le A \le 0.14$ to ensure small-amplitude perturbations for promoting a linear instability during the transition to turbulence (Schmid & Henningson 2001). It is also important to note that, due to the addition of a global artificial diffusion and use of spectral method, it is almost unachievable to trigger transition to turbulence for Re < 2000, even with a sufficiently large perturbation amplitude A > 0.14.

Prior to proceeding to the results, it is worth emphasizing the flow regime of the current study. For El < 0.02 and $2000 \le Re \le 5000$, the flow regime of interest can be referred to as inertia-driven transition for both Newtonian and dilute viscoelastic flows (Datta *et al.* 2022). The EIT flow regime, which is typically $El \gg 0.02$ (Dubief *et al.* 2013; Samanta *et al.* 2013), is distinctly different from the current flow regime. Thus, a quantitative or even qualitative comparison between the current inertia-driven transition and EIT transition should not necessarily be expected in the following results.

3. Results and discussion

We perform direct numerical simulations starting from a laminar base flow disturbed with a small finite-amplitude perturbation for both Newtonian and viscoelastic flows. The amplitude of the perturbation was set to be in the range of $0.014 \le A \le 0.14$ relative to the total energy of the laminar base flow.

3.1. Transition dynamics

To examine the temporal behaviour of the transition dynamics, figure 1(a) illustrates the evolution of the disturbance energy per unit volume E(t), which is given as

$$E(t) = \frac{1}{2L_x L_z} \int_0^{L_z} \int_{-1}^1 \int_0^{L_x} (u'^2 + v'^2 + w'^2) \, \mathrm{d}x \, \mathrm{d}y \, \mathrm{d}z, \tag{3.1}$$

where the streamwise velocity fluctuation $u' = u - u_{lam}$, while v' = v and w' = w since $v_{lam} = 0$ and $w_{lam} = 0$. Profiles are normalized by the initial disturbance energy E_0 . At t=0, the same amplitude of perturbation A=0.07 was applied to both Newtonian and viscoelastic (c = 0.03 or $\beta = 0.97$) flows at Re = 2500. As has been typically observed in transition to turbulence (Schmid & Henningson 2001), both flows exhibit a similar early-time behaviour of the energy growth: (i) an initial stable period, (ii) a sharp increase up to the maximum value, or namely a strong burst, and (iii) transition to a fully turbulent flow. However, the first notable distinction between both flows is the duration of the initial stable period. As clearly seen in figure 1(a), the viscoelastic flow experiences a shorter stable duration than the Newtonian counterpart. In other words, polymers appear to destabilize the flow earlier than the Newtonian flow, triggering an earlier transition. Another distinction lies in the strong burst whose magnitude is significantly reduced by polymers. This strong burst has also been referred to as the escaping process out of the so-called exact coherent solution along its most unstable manifold (Itano & Toh 2001; Park, Shekar & Graham 2018), comprising the linearly unstable stage followed by the nonlinear evolution stage. A log-linear representation of the evolution of the disturbance energy per unit volume E(t) is shown in figure 1(b). The exponential amplification of the perturbations in both Newtonian and viscoelastic flows is marked by dotted lines with σ values equal to 0.06 and 0.05 for Newtonian and viscoelastic flows, respectively. After the strong burst, both flows enter a fully turbulent regime at $t \approx 150$, where turbulent DR via polymers is manifested.

To further characterize the transition to turbulence, we utilize the mean wall shear stress τ_w as a means to estimate the transitional trajectory of Newtonian and viscoelastic flows, as it has been widely utilized to characterize the intermittent dynamics of both flows (Xi & Graham 2012). The top panels in figure 2 show the temporal evolution of the wall shear stress for Newtonian and viscoelastic flows of various polymer concentrations perturbed with A = 0.07 at Re = 2000, 2500 and 3000 along with the base laminar state whose wall shear stress $\tau_{w,lam} = 2$. The response of the flow to the perturbation can be divided in two distinct cases: (a) the flow remains undisturbed or (b) the flow departs from the base laminar state and begins its path to turbulence shortly after the introduction of the perturbation. For Re = 2000 (figure 2a), the Newtonian flow remains undisturbed (case a), whereas the viscoelastic flows of all polymer concentrations begin transition at a few time instants after the introduction of the perturbation (case b). For $Re \ge 2500$, both Newtonian and viscoelastic flows follow a transition trajectory (case b). As clearly seen in figure 2(b), the transition begins at an earlier time for viscoelastic flows than for their Newtonian counterpart, indicating an earlier transition. At a higher Reynolds

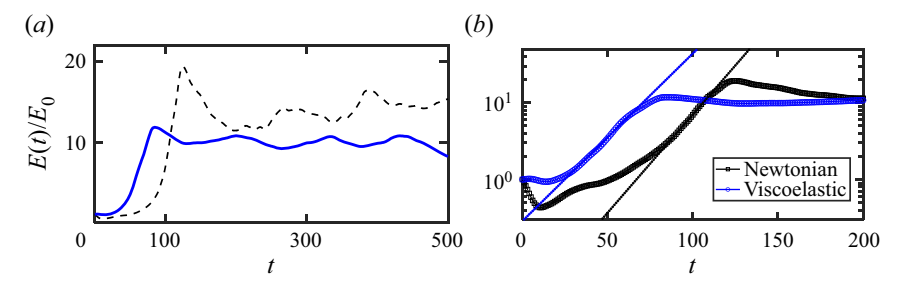


Figure 1. Temporal evolution of the disturbance energy E(t) normalized by the initial disturbance energy E_0 on (a) a linear–linear scale and (b) a log–linear scale for Newtonian (black dashed line/squares) and viscoelastic flows $(c=0.03 \text{ or } \beta=0.97; \text{ blue solid line/circles})$. Both flows are disturbed by the perturbation amplitude A=0.07 at Re=2500. The amplification of the perturbation (straight lines in b) behaves like $e^{\sigma t}$, where $\sigma=0.06$ and 0.05 for Newtonian and viscoelastic flows, respectively.

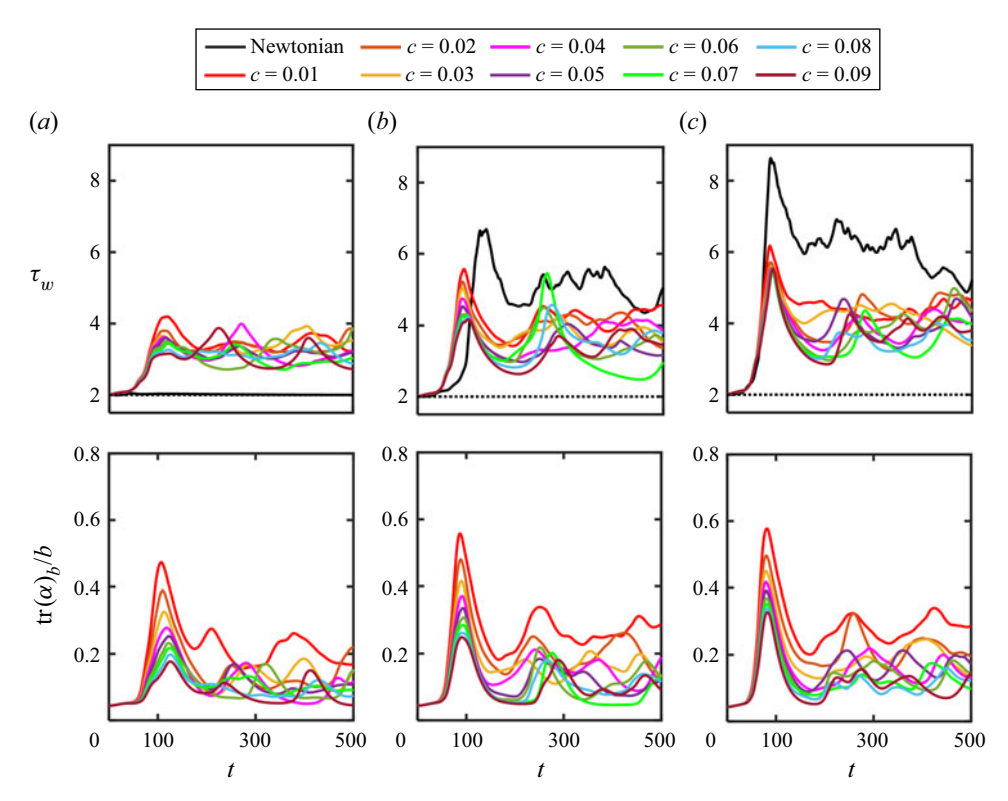


Figure 2. Temporal evolution of the (top panel) wall shear stress τ_w and (bottom panel) bulk polymer stretching normalized by the maximum extensibility of polymers $tr(\alpha)_b/b$ for the perturbation amplitude A=0.07 at (a) Re=2000 (b) Re=2500 and (c) Re=3000: laminar state (black dashed line), Newtonian flow (black solid line) and viscoelastic flows of various polymer concentrations (coloured solid lines).

number of Re = 3000 (figure 2c), however, the transition appears to begin at almost the same time for Newtonian and viscoelastic flows. Similar to the perturbation energy in figure 1(a), the maximum wall shear stress of the strong burst in viscoelastic flows is smaller than the one in Newtonian flow. Furthermore, the maximum wall shear stress is reduced with increasing polymer concentration, implying that the magnitude of the

A. Martinez Ibarra and J.S. Park

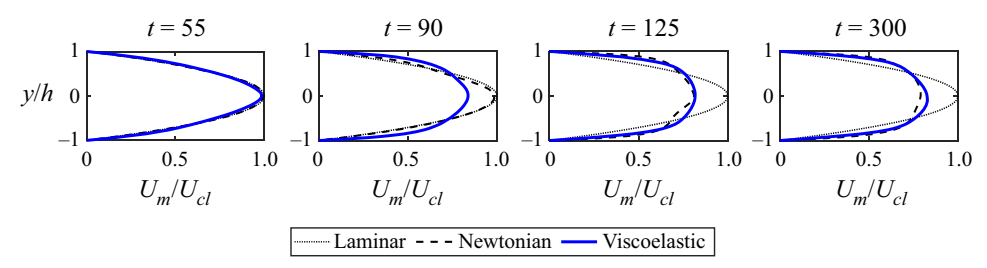


Figure 3. Temporal evolution of the mean velocity profile U_m normalized by the laminar centreline velocity U_{cl} for the perturbation amplitude A=0.07 at Re=2500 with the time instants t=55, 90, 125 and 300: laminar state (black dotted line), Newtonian flow (black dashed line) and viscoelastic flow (c=0.03; blue solid line).

strong burst decreases with polymer concentration. The reduction of the aforementioned maximum wall shear stress of the polymer solutions is also an important indicator of DR in sustained turbulent flow regimes. Hence, turbulent DR is expected for viscoelastic flows compared with Newtonian counterparts, as can be seen in the wall shear stress in figure 2(b,c). The bottom panels in figure 2 show the temporal evolution of the bulk polymer stretching $tr(\alpha)_b$ normalized by the maximum extensibility of polymers b for various polymer concentrations. Interestingly, the bulk polymer stretching of all polymer concentrations is almost identical and increases very slowly until a sharp increase begins at almost the same time as the wall shear stress starts to increase sharply.

As an alternative to characterize the transition to turbulence, the distortion of the mean velocity profile has also been utilized for Newtonian flows, as its relationship to the formation of vortical structures during transition has been well established (Lemoult et al. 2012). Figure 3 shows snapshots of the mean velocity profile U_m normalized by the Newtonian laminar centreline velocity U_{cl} at Re = 2500 at four different time instants for Newtonian and viscoelastic (c = 0.03) flows along with the base laminar profile as a reference. At t = 55, the velocity profile of both flows appears to be close to the base laminar profile. At the peak of the strong burst for the viscoelastic flow (t = 90), the deformation of the mean velocity profile is evident, while its Newtonian counterpart remains almost unchanged up to t = 100. At the peak of the strong burst for the Newtonian flow (t = 125), however, a severe deviation from the laminar profile is observed for both flows. Once the fully turbulent state is reached (t = 300), the viscoelastic profile is closer to the laminar profile, suggesting drag reduction by polymers. For a further investigation, figure 4 shows the temporal evolution of the peak velocity U_{peak} normalized by the centreline velocity U_{cl} for Newtonian and viscoelastic flows of various polymer concentrations at Re = 2000, 2500 and 3000 perturbed with A = 0.07. The base laminar state is also included, for which $U_{peak}/U_{cl} = 1$. Similarly, the response of the flow can be equally distinguished by cases (a) and (b) when utilizing U_{peak}/U_{cl} . For Re = 2000(figure 4a), the Newtonian flow departs slightly from the laminar state; however, the transition is not achieved and the flow remains laminar (case a), whereas the viscoelastic flows of all polymer concentrations deviate from the laminar state and continue the transitional path to turbulence (case b). Once the transition to turbulence is established, the velocity ratio quickly decreases until a fully turbulent state is reached. For $Re \ge 2500$, both Newtonian and viscoelastic flows respond following the path of case (b). The earlier departure from the laminar state ratio of 1 is clearly observed for viscoelastic flows in figure 4(b), as in the wall shear stress (figure 2b). The similarity in the start of transition in Newtonian and viscoelastic flows at Re = 3000 can also be confirmed by figure 4(c).

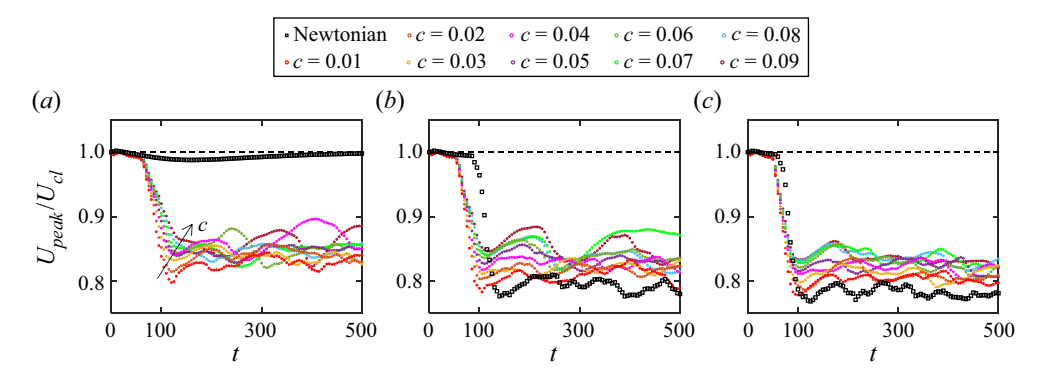


Figure 4. Temporal evolution of the peak velocity normalized by the laminar centreline velocity for the perturbation amplitude A = 0.07 at (a) Re = 2000, (b) Re = 2500 and (c) Re = 3000: laminar state (black dashed line), Newtonian flow (black squares) and viscoelastic flow of various polymer concentrations (coloured symbols).

3.2. Transition time: onset of transition

Now, we proceed to investigate the time for the onset of transition. The transition time T_t is defined as the time at which the wall shear stress reaches 105% of the base laminar value ($\tau_w = 2.1$). The sensitivity to the chosen threshold value was examined by utilizing different threshold values, such as 110% and 115%, showing almost identical trends with an upward shift in the time it takes for each case to reach the threshold criteria. In addition, the sensitivity to the chosen parameter was also examined by utilizing the peak velocity, such as figure 4, with the threshold of 95% of the base laminar value, showing an almost identical trend. It should be noted that the aforementioned criteria for the onset of transition can only be detected in cases where the perturbation amplitude is strong enough to trigger transition for both Newtonian and viscoelastic flows.

Figure 5 shows the transition time for Newtonian and viscoelastic flows of various polymer concentrations at Reynolds numbers up to 5000 as a function of perturbation amplitude. As expected, the overall trend appears to be similar for both Newtonian and viscoelastic flows, where the transition time decreases with increasing perturbation amplitude and Reynolds number. The earlier transition for viscoelastic flows is also confirmed by a smaller T_t regardless of polymer concentration (i.e. transition is initiated at an earlier time than Newtonian flow). Interestingly, it seems that the polymer concentration has a negligible effect on the transition time for all Re. Yet, as clearly observed in all Reynolds numbers studied, the main difference is that the viscoelastic flow requires a lower perturbation amplitude to trigger the transition in comparison with its Newtonian counterpart. For example, figure 5(a) shows that, at Re = 2000, the lowest or critical perturbation amplitudes to trigger transition are $A \approx 0.08$ and $A \approx 0.05$ for the Newtonian and viscoelastic flows, respectively. Increasing the Reynolds number lowers the critical perturbation amplitude for both Newtonian and viscoelastic flows. In addition, the difference between the Newtonian and viscoelastic transition times ΔT_t gets smaller with increasing Re. In order to better explore the effect of Reynolds number, we replot the transition time as a function of Reynolds number at a given perturbation amplitude, as shown in figure 6. For viscoelastic flows, the polymer concentration c = 0.03 is only used as the polymer concentration appears to have no impact on the transition time. At three perturbation amplitudes considered, the transition time decreases monotonically for both flows with increasing Reynolds number. For a relatively weak perturbation amplitude A = 0.07 (figure 6a), $\Delta T_t \approx 6$ and this value remains almost constant with increasing

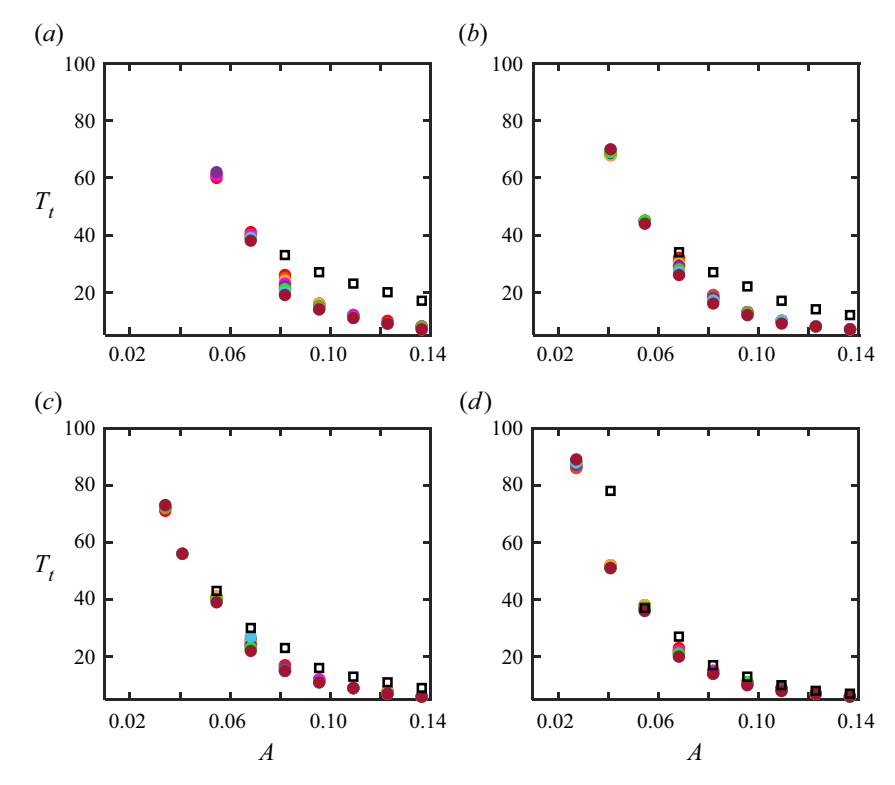


Figure 5. Transition time as a function of perturbation amplitude A at (a) Re = 2000, (b) Re = 3000, (c) Re = 4000 and (d) Re = 5000: Newtonian flow (black open squares) and viscoelastic flow of various polymer concentrations (coloured solid circles). Refer to the legend in figure 2 for colours for polymer concentration.

Reynolds number. However, for relatively strong perturbation amplitudes of A > 0.07 (figure 6b,c), ΔT_t becomes more significant for lower Reynolds numbers but gets much smaller with increasing Reynolds number. For A = 0.12 (figure 6c), the transition time of the viscoelastic flow barely decreases with Reynolds number, and ΔT_t is almost negligible at Re = 5000. It is worth noting that, at the given Reynolds number, the transition time decreases with the perturbation amplitude. However, the level of DR achieved by the same polymer parameters during sustained turbulence would be very similar and insensitive to the transition time.

3.3. Stability curve: critical perturbation amplitude

Next, we present the finite-amplitude thresholds for the perturbation to start triggering the transition or the critical perturbation amplitude A_c below which no transition occurs. Figure 7 shows A_c for Newtonian and viscoelastic (c=0.03) flows on a log-log scale. As expected from the previous studies for Newtonian flows (e.g. Hof *et al.* 2003; Lemoult *et al.* 2012), our Newtonian flow (black open squares) clearly follows a power-law scaling of Re^{γ} for $Re \ge 2500$. As was observed by Lemoult *et al.* (2012), it is also observed that the asymptotic regime is not reached at lower Reynolds numbers for Re < 2500. The critical exponent γ for the Newtonian flow is very close to -1.25, which has also been reported for transition in PPF triggered by a perturbation leading to streamwise vortices (Chapman 2002). Most interestingly, the viscoelastic flow also follows almost the same

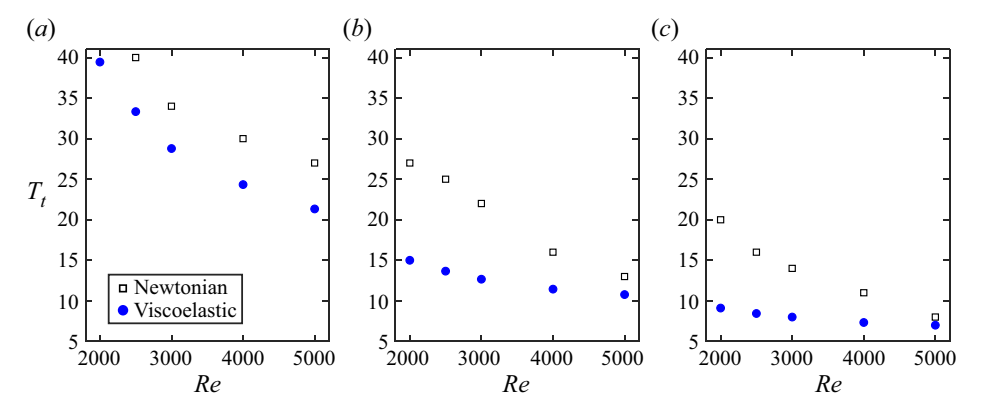


Figure 6. Transition time as a function of Reynolds number Re for the perturbation amplitude (a) A = 0.07, (b) A = 0.10 and (c) A = 0.12 for Newtonian flow (black open squares) and viscoelastic flow (c = 0.03; blue solid circles).

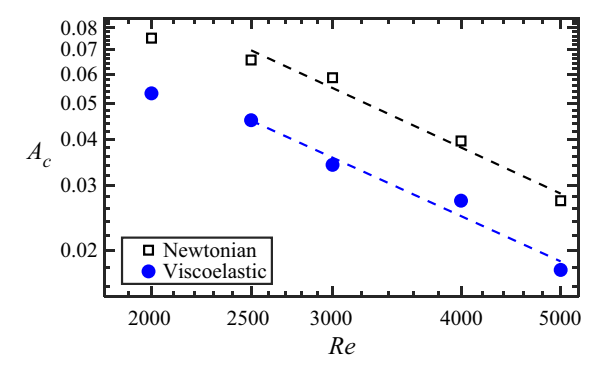


Figure 7. Log-log plot of the stability curve for the onset of transition to turbulence in the range of $2000 \le Re \le 5000$. Newtonian flow (black open squares) and viscoelastic flow (c = 0.03) (blue solid circles). For $Re \ge 2500$, the minimum or critical perturbation amplitude A_c follows a power-law scaling of $A_c = O(Re^{\gamma})$, where $\gamma \approx -1.25$ for both Newtonian and viscoelastic flows.

power-law scaling as the Newtonian flow with $\gamma \approx -1.25$ for $Re \geq 2500$. It can also be observed that the viscoelastic A_c is smaller than the Newtonian A_c , which suggests that smaller finite perturbation amplitudes are sufficient to trigger transition for viscoelastic flows compared with their Newtonian counterparts. It should be noted that the same scaling law with a constant exponent is found for different perturbation fields generated by Channelflow, while the asymptotic lines are shifted upward or downward depending on the characteristics of the perturbation structure (see the Appendix).

For a comprehensive understanding of transition to turbulence and a direct comparison between Newtonian and viscoelastic flows, figure 8(a,b) presents the state diagram of the transition time T_t in a space of the perturbation amplitude A and Reynolds number Re for Newtonian and viscoelastic (c = 0.03) flows, respectively. As can be seen, there are two distinct regions, laminar and turbulent, separated by the laminar–turbulent boundary (thick black line) separating the basins of attraction of laminar and turbulent flows (Schneider, Eckhardt & Yorke 2007; Duguet, Willis & Kerswell 2008). This boundary indeed represents the critical perturbation amplitude A_c in figure 7. Since there are theoretical arguments that the so-called exact coherent states (ECSs) form a part of the

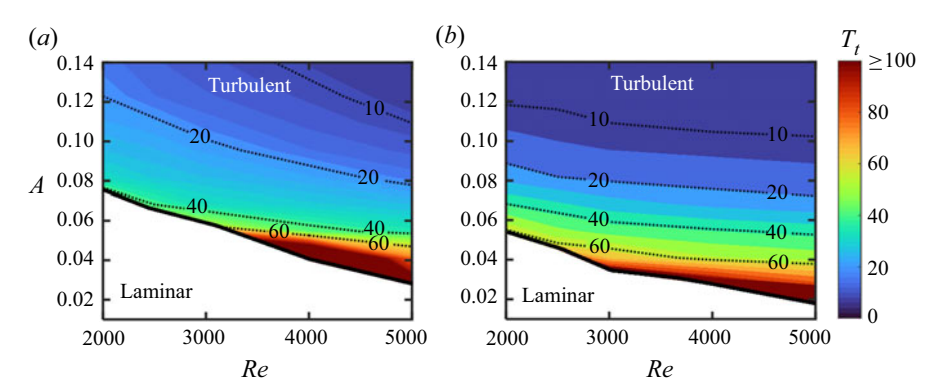


Figure 8. Colour contour of the transition time T_t due to a finite amplitude of the perturbation A at Reynolds number Re for (a) Newtonian flow and (b) viscoelastic (c = 0.03) flow. The thick black line separates the basins of attraction of laminar and turbulent flows.

basin boundary (Kawahara 2005; Wang, Gibson & Waleffe 2007), the dynamics on or near this boundary could play an important role in finding new ECSs in viscoelastic flows or EIT (Page *et al.* 2020; Buza *et al.* 2022; Dubief *et al.* 2022), which will be a subject of interesting future work.

Clearly, this boundary is shifted down for the viscoelastic flow, suggesting that the laminar region is shrunk by polymers. It also suggests the reduction in the perturbation magnitude required to trigger transition for viscoelastic flows. A shorter transition time of the viscoelastic flow can be readily identified in comparison with the Newtonian flow at the given Reynolds number and perturbation amplitude. Interestingly, the decay rate of the transition time with respect to the Reynolds number shows distinct trends. As can be seen in lines of constant T_t values from 60 to 10, the slope of these lines gets steeper for the Newtonian flow, while the lines level off for the viscoelastic flow. This could suggest that, at very high perturbation amplitudes, the effect of polymers on the transition time or the early stage of transition is almost the same, regardless of Reynolds number, which can also be confirmed by figure 6(c).

3.4. Mechanism: velocity fluctuations, flow structures and polymer dynamics

We now attempt to elucidate the mechanisms behind the earlier transition triggered by polymers in viscoelastic flows. Figure 9(a) shows the evolution of the wall shear stress at Re = 2500 for Newtonian and viscoelastic (c = 0.03) flows at four different time instants. Figure 9(b-d) shows snapshots of the velocity fluctuations in the streamwise u_{rms} , wall-normal v_{rms} and spanwise w_{rms} directions at each time instant for both flows. An observation to draw from figure 9(c,d) at t = 55 is that changes in the wall-normal velocity fluctuation v_{rms} and spanwise velocity fluctuation w_{rms} in the viscoelastic flow, with respect to its Newtonian counterparts, are somewhat more significant compared with the streamwise velocity fluctuation u_{rms} . For the Newtonian case, v_{rms} is significantly lower near the wall and w_{rms} is barely observed compared with ones for the viscoelastic flow. This suggests that the wall-normal and spanwise directions are destabilized earlier by polymers, eventually promoting an earlier transition. In other words, an early transition observed in the viscoelastic flow is attributed to the early destabilization of the wall-normal and spanwise directions due to polymers. As the transition process proceeds, v_{rms} and v_{rms} of the Newtonian flow take over and continue to be larger than those of the

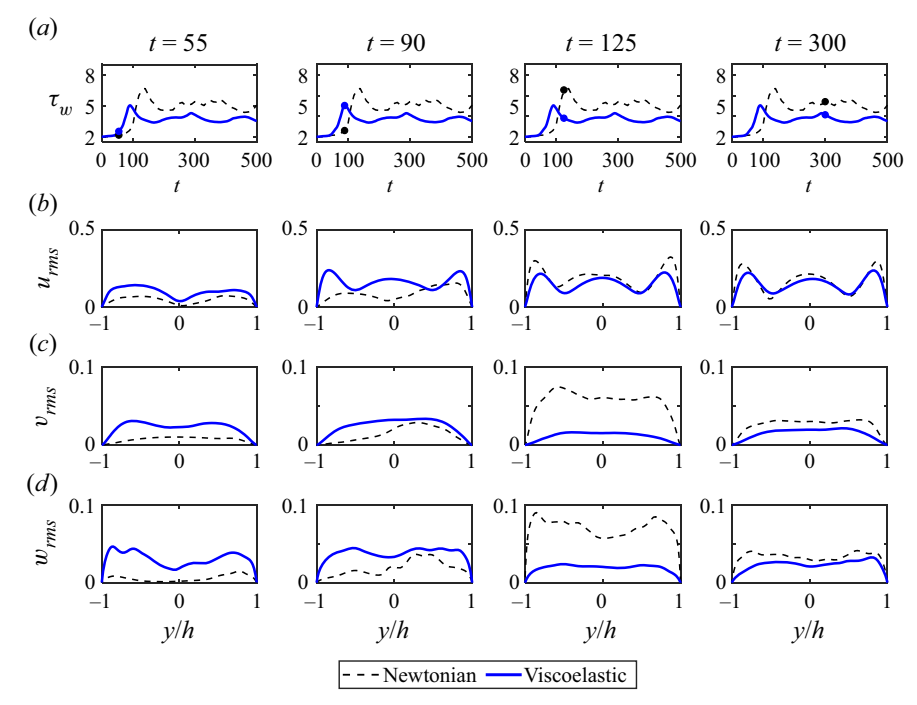


Figure 9. (a) Temporal evolution of the wall shear stress τ_w at Re = 2500 for the perturbation amplitude A = 0.07 for Newtonian flow (black dashed line) and viscoelastic flow (c = 0.03; blue solid line) with the time instants t = 55, 90, 125 and 300. Snapshots of the (b) streamwise, (c) wall-normal and (d) spanwise velocity fluctuations at each time instant shown in (a). Also see the accompanying supplementary movie available at https://doi.org/10.1017/jfm.2023.930.

viscoelastic flow. Once the transitional period of both flows has passed (t = 300), a fully sustained turbulent regime begins, where the expected characteristics of the drag-reduced flow are observed such that v_{rms} and w_{rms} of the viscoelastic flow are lower than those of the Newtonian flow (Li *et al.* 2006). This whole process can be seen in the accompanying supplementary movie.

This destabilization mechanism is further studied by estimating the effect of viscoelasticity on flow structures. Vortex identification is performed by utilizing the so-called Q-criterion (Jeong & Fazle 1995) for which $Q = \frac{1}{2}(\|\Omega\|^2 - \|S\|^2)$ is computed, where $S \equiv \frac{1}{2}(\nabla u + \nabla u^T)$ is the rate of strain tensor and $\Omega \equiv \frac{1}{2}(\nabla u - \nabla u^T)$ is the vorticity tensor. Regions of Q > 0 correspond to the areas of strong vortical motions. Figure 10 shows snapshots of these vortical structures for the lower half of the channel for Newtonian flow (a-d) and viscoelastic flows of c = 0.03 (e-h) at different time instants that can also be seen in the evolution of wall shear stress in figure 9(a). The red tubes represent isosurfaces of Q = 0.216, which is approximately half of the maximum of the sustained viscoelastic turbulent flow for this particular case. For comparison, the half of the maximum of the sustained Newtonian turbulent flow is Q = 2.21. The blue contours correspond to isosurfaces of constant streamwise velocity, which could represent a spatial structure for the streak.

Figure 10(a,e) shows the flow structures at the beginning stage of the transition process (t = 55) for Newtonian and viscoelastic flows, respectively. As polymers destabilize the flow earlier which results in rapid energy growth, the streamwise-elongated red tubes or

A. Martinez Ibarra and J.S. Park

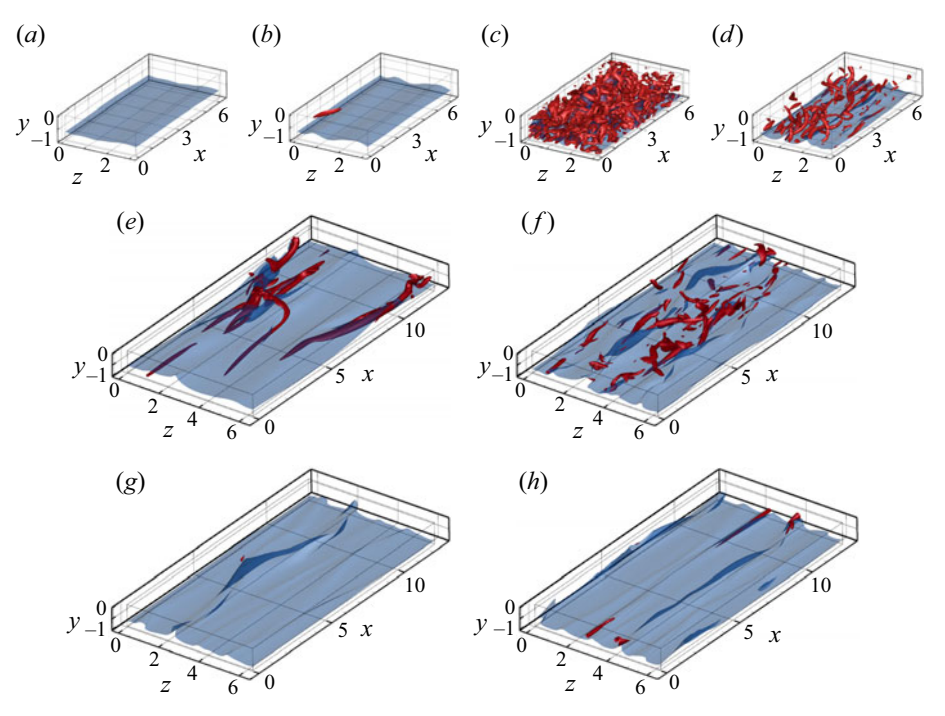


Figure 10. Temporal evolution of vortical structures for the bottom half-channel: (a-d) for Newtonian and (e-h) viscoelastic (c=0.03) flows at Re=2500 triggered by the perturbation amplitude A=0.07. The red tubes are isosurfaces at constant vortex strength Q=0.216, and the blue contours are isosurfaces of constant streamwise velocity. The maximum strengths are (a) 0.018, (b) 1.29, (c) 14.64, (d) 4.25, (e) 4.49, (f) 2.39, (g) 0.25 and (h) 0.63. For reference, the maximum vortex strengths for sustained turbulence are Q=4.42 and Q=0.48 for Newtonian and viscoelastic flows, respectively. Also see the accompanying supplementary movies. (a,e) t=55, (b,f) t=90, (c,g) t=125 and (d,h) t=300.

quasi-streamwise vortices start to form around wavy, uplifted blue isosurfaces, whereas its Newtonian counterpart remains undisturbed. This wavy, uplifted structure indeed signifies the form of low-speed streaks, which is one of the key ingredients for the self-sustaining process (Waleffe 1997). It should be noted that, given the flow regime of the current study, the spanwise-oriented structures that are predominantly observed in the EIT regime are unlikely to be observed. As the viscoelastic flow reaches its bursting peak at t = 90, figure 10(f) shows a relatively larger population of vortex cores formed around more enhanced low-speed streaks. After the bursting peak, the vortices are then quickly dampened as polymers work against them, entering a drag-reduced turbulent regime (figure 10h at t = 300). In comparison, when its Newtonian counterpart reaches its bursting peak at t = 125 (figure 10c), more heavily populated vortex cores are formed across almost the entire domain, where the characteristics of the vortical structures are hard to identify. After the strong bursting peak, however, some of the quasi-streamwise vortices are observed as seen in figure 10(d).

In addition to the velocity fluctuations and flow structures, the polymer dynamics can also provide the underlying mechanism behind the early transition. As the more stretched polymer state ties into the more unstable flow state (Xi & Graham 2010; Graham 2014), we can refer to the bulk polymer stretching in figure 2. In the early transition stage, the polymers start to stretch slowly as they interact with the flow. As they keep stretching, polymers continue to destabilize the flow to enhance the velocity fluctuations.

The transition eventually occurs when the bulk polymer stretching reaches a certain value, depending on the Reynolds number and perturbation amplitude, after which the bulk polymer stretching starts to increase sharply, as seen in figure 2.

In short, the destabilization mechanism of polymers during transition is attributed to the early amplification of the wall-normal and spanwise velocity fluctuations and the formation of the quasi-streamwise vortices around a low-speed streak, all of which facilitate an early transition. Interestingly, the vortical structures observed in both Newtonian and viscoelastic flows also support the power exponent $\gamma = -1.25$ in the power-law scaling of the critical perturbation amplitude in figure 7, as also observed in the previous study (Chapman 2002). It should be noted, however, that a perturbation leading to different flow structures could provide a power-law scaling with a different exponent. In addition, this study focuses on a dilute polymer solution (c < 0.1) and low elasticity (El < 0.02), where only an early transition is observed. Thus, it could suggest a subject of future work for the transition to turbulence in polymer solutions at semi-concentrated or highly concentrated regimes above the overlap concentration and at high elasticity ($El \gg 0.02$) such as within the EIT regime, where different transition scenarios or flow structures could arise (Datta *et al.* 2022).

4. Conclusion

Direct numerical simulations of dilute polymer solutions with a FENE-P model were performed to investigate the effect of polymers on the laminar-turbulent transition in plane Poiseuille (channel) flow. Starting from a base laminar state, which is disturbed with a small finite-amplitude perturbation, the short stable period was observed for both Newtonian and viscoelastic flows at the beginning followed by the linear and nonlinear evolution of the disturbance energy. However, the viscoelastic flow experiences a shorter duration of the stable period, hinting at a destabilizing effect of the polymers during the early stages of transition. Also, we observed that the viscoelastic flow requires a smaller amplitude of perturbation to trigger transition, whereas the Newtonian counterpart remains undisturbed until a larger amplitude is utilized to trigger transition. We show that the transition time T_t , defined as the onset time of transition, decreases with increasing perturbation amplitude. As polymers promote an early transition, the Newtonian flow exhibits a higher T_t than the viscoelastic flow, but this difference becomes less pronounced as Re is increased. Interestingly, the polymer concentration studied (0.01 < c < 0.09)barely has an effect on the transition time. However, the higher the polymer concentration, the lower the magnitude of the strong burst, suggesting that higher polymer concentrations exhibit enhanced drag-reducing behaviour after the onset of transition.

We then investigated the critical perturbation amplitude A_c , which is the minimum amplitude to trigger the transition. The viscoelastic flow shows a smaller A_c than its Newtonian counterpart, suggesting that polymers kick in the destabilizing effect early. Similar to previous studies for Newtonian transition, the critical amplitude of our Newtonian flow follows a power-law scaling of Re^{γ} for $Re \geq 2500$, where $\gamma \approx -1.25$. More interestingly, a viscoelastic flow also follows almost the identical power-law scaling as the Newtonian flow. Both flows display almost the same critical exponent of $\gamma \approx -1.25$ for $Re \geq 2500$. This critical exponent implies that the perturbation of the current study leads to the formation of quasi-streamwise vortices (Chapman 2002).

The early transition or destabilization effect triggered by polymers is further investigated. During the stable period at the beginning stage of transition, the wall-normal and spanwise velocity fluctuations start to grow early in the viscoelastic flow, compared with those of the Newtonian flow. Hence, the polymers appear to destabilize these

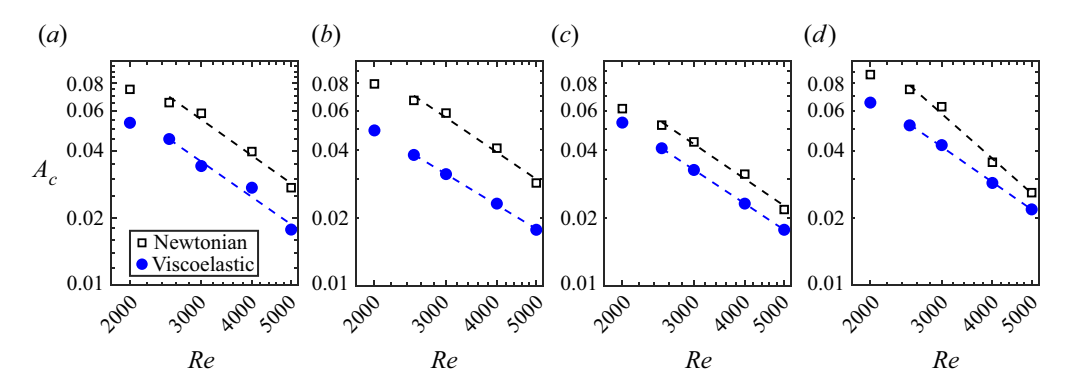


Figure 11. Log-log plot of the stability curve for the onset of transition to turbulence in the range of $2000 \le Re \le 5000$ of the different perturbations: (a) form I (current study), (b) form II, (c) form III and (d) form IV. Each form is meant to display different vortical structures in terms of the strength and shape. Newtonian flow (black open squares); viscoelastic flow (c = 0.03) (blue solid circles). For $Re \ge 2500$, the minimum or critical perturbation amplitude A_c follows a power-law scaling of $A_c = O(Re^{\gamma})$, where $\gamma \approx -1.25$ for all the cases, except for a Newtonian case in form IV of $\gamma \approx -1.50$.

components of the velocity fluctuation quickly, promoting an earlier transition. Once the fully turbulent stage is reached after the strong burst, however, the drag-reducing behaviour of polymers is observed, where the wall-normal and spanwise velocity fluctuations for the viscoelastic flow are reduced and become smaller than those of the Newtonian flow. This destabilizing effect of polymers was also confirmed by considering the bulk polymer stretching and visualizing the flow structure, where the vortical motions are shown up earlier around low-speed streaks for a viscoelastic flow. Interestingly, it is possible to see the formation of quasi-streamwise vortices for both flows, which supports the critical exponent of $\gamma \approx -1.25$ for the power-law scaling of the critical amplitude.

This study further complements the previous studies on the laminar-turbulent transition by providing the power-law scaling of the critical perturbation amplitude for both Newtonian and viscoelastic flows, which has been mostly unexplored. The destabilizing effect of polymers during the early stage of transition is consistent with the effects of a low elasticity number and polymer concentration, as is the case of our study. Moving forward, the robustness of the power-law scaling on different perturbation structures should be further investigated. Additionally, higher elasticity numbers and polymer concentrations may lead to different transition dynamics and mechanisms, which will be a subject of interesting future work.

Supplementary movies. Supplementary movies are available at https://doi.org/10.1017/jfm.2023.930.

Acknowledgements. The direct numerical simulation code used was developed and distributed by J. Gibson at the University of New Hampshire. The authors also acknowledge the computing facilities used at the Holland Computing Center at the University of Nebraska-Lincoln.

Funding. Research is supported by the US Department of Energy, Office of Science, Office of Basic Energy Sciences under award number DE-SC0022280 (modelling studies) and by the National Science Foundation under award numbers OIA-1832976 and CBET-2142916 (CAREER) (computational studies).

Declaration of interests. The authors report no conflict of interest.

Author ORCIDs.

Jae Sung Park https://orcid.org/0000-0002-7966-1164.

Appendix. Different perturbation forms

Figure 11 shows the critical perturbation amplitude A_c for Newtonian and viscoelastic (c=0.03) flows on a log-log scale for various perturbation forms, where form I is the perturbation used in the current study. These perturbations were generated by Channelflow, which allows us to create different forms of the perturbation field in terms of different vortical structures and strengths. It is observed that the same power-law scaling of $A_c = O(Re^{\gamma})$ with $\gamma \approx -1.25$ is found for both Newtonian and viscoelastic flows with all perturbation forms studied for $Re \ge 2500$, while asymptotic lines are shifted upward or downward depending on different perturbation forms. It should be noted, however, that a Newtonian flow of form IV exhibits a slightly higher exponent of $\gamma \approx -1.50$. Although the different forms of the perturbation lead to the same stability scaling, a detailed analysis of the transition dynamics due to each different perturbation form is necessary but beyond the scope of the current study, and will be a subject of future work.

REFERENCES

- AGARWAL, A., BRANDT, L. & ZAKI, T.A. 2014 Linear and nonlinear evolution of a localized disturbance in polymeric channel flow. *J. Fluid Mech.* **760**, 278–303.
- AGARWAL, A., BRANDT, L. & ZAKI, T.A. 2015 Transition to turbulence in viscoelastic channel flow. *Proc. IUTAM* 14, 519–526.
- AVILA, M., BARKLEY, D. & HOF, B. 2023 Transition to turbulence in pipe flow. *Annu. Rev. Fluid Mech.* 55, 575–602.
- BIANCOFIORE, L., BRANDT, L. & ZAKI, T.A. 2017 Streak instability in viscoelastic Couette flow. *Phys. Rev.* F **2**, 043304.
- BIRD, R.B., CURTISS, C.F., ARMSTRONG, R.C. & HASSAGER, O. 1987 Dynamics of Polymeric Liquids, vol. 2, 2nd edn. John Wiley & Sons.
- BOBERG, L. & BROSA, U. 1988 Onset of turbulence in a pipe. Z. Naturforsch. A 43, 697-726.
- BOUCHENAFA, W., DEWALS, B., LEFEVRE, A. & MIGNOT, E. 2021 Water soluble polymers as a means to increase flow capacity: field experiment of drag reduction by polymer additives in an irrigation canal. *J. Hydraul. Engng* 147, 05021003.
- BUTLER, K.M. & FARRELL, B.F. 1992 Three-dimensional optimal perturbations in viscous shear flow. *Phys. Fluids* A **4**, 1637–1650.
- BUZA, G., BENEITEZ, M., PAGE, J. & KERSWELL, R.R. 2022 Finite-amplitude elastic waves in viscoelastic channel flow from large to zero Reynolds number. *J. Fluid Mech.* **951**, 1–21.
- CARLSON, D.R., WIDNALL, S.E. & PEETERS, M.F. 1982 A flow-visualization study of transition in plane Poiseuille flow. J. Fluid Mech. 121, 487–505.
- CASTILLO-SÁNCHEZ, H.A., JOVANOVIĆ, M.R., KUMAR, S., MOROZOV, A., SHANKAR, V., SUBRAMANIAN, G. & WILSON, H.J. 2022 Understanding viscoelastic flow instabilities: Oldroyd-B and beyond. *J. Non-Newtonian Fluid Mech.* 302, 104742.
- CHANDRA, B., SHANKAR, V. & DAS, D. 2018 Onset of transition in the flow of polymer solutions through microtubes. J. Fluid Mech. 844, 1052–1083.
- CHAPMAN, S.J. 2002 Subcritical transition in channel flows. J. Fluid Mech. 451, 35–97.
- CHAUDHARY, I., GARG, P., SUBRAMANIAN, G. & SHANKAR, V. 2021 Linear instability of viscoelastic pipe flow. J. Fluid Mech. 908, A11.
- CHERUBINI, S. & PALMA, P.D. 2013 Nonlinear optimal perturbations in a Couette flow: bursting and transition. *J. Fluid Mech.* **716**, 251–279.
- CHOUEIRI, G.H., LOPEZ, J.M. & HOF, B. 2018 Exceeding the asymptotic limit of polymer drag reduction. Phys. Rev. Lett. 120, 124501.
- CRUZ, D.O.A., PINHO, F.T. & OLIVEIRA, P.J. 2005 Analytical solutions for fully developed laminar flow of some viscoelastic liquids with a Newtonian solvent contribution. J. Non-Newtonian Fluid Mech. 132, 28–35.
- DARBYSHIRE, A.G. & MULLIN, T. 1995 Transition to turbulence in constant-mass-flux pipe flow. J. Fluid Mech. 289, 83–114.
- DATTA, S.S., et al. 2022 Perspectives on viscoelastic flow instabilities and elastic turbulence. Phys. Rev. F 7, 080701.

A. Martinez Ibarra and J.S. Park

- DAUCHOT, O. & DAVIAUD, F. 1995 Finite amplitude perturbation and spots growth mechanism in plane Couette flow. *Phys. Fluids* 7 (2), 335–343.
- DAVIES, S.J. & WHITE, C.M. 1928 An experimental study of the flow of water in pipes of rectangular section. *Proc. R. Soc. Lond.* A **119**, 92–107.
- DIMITROPOULOS, C.D., SURESHKUMAR, R. & BERIS, A.N. 1998 Direct numerical simulation of viscoelastic turbulent channel flow exhibiting drag reduction: effect of the variation of rheological parameters. *J. Non-Newtonian Fluid Mech.* 79, 433–468.
- DRAAD, A.A., KUIKEN, G.D.C. & NIEUWSTADT, F.T.M. 1998 Laminar-turbulent transition in pipe flow for Newtonian and non-Newtonian fluids. *J. Fluid Mech.* **377**, 267–312.
- DRAZIN, P.G. & REID, W.H. 1981 Hydrodynamic Stability. Cambridge University Press.
- DUBIEF, Y., PAGE, J., KERSWELL, R.R., TERRAPON, V.E. & STEINBERG, V. 2022 First coherent structure in elasto-inertial turbulence. *Phys. Rev. Fluids* 7, 073301.
- DUBIEF, Y., TERRAPON, V.E. & SORIA, J. 2013 On the mechanism of elasto-inertial turbulence. *Phys. Fluids* **25**, 110817.
- DUGUET, Y., MONOKROUSOS, A., BRANDT, L. & HENNINGSON, D.S. 2013 Minimal transition thresholds in plane Couette flow. *Phys. Fluids* **25** (8), 084103.
- DUGUET, Y., WILLIS, A.P. & KERSWELL, R.R. 2008 Transition in pipe flow: the saddle structure on the boundary of turbulence. *J. Fluid Mech.* **613**, 255–274.
- ECKHARDT, B., SCHNEIDER, T.M., HOF, B. & WESTERWEEL, J. 2007 Turbulence transition in pipe flow. *Annu. Rev. Fluid Mech.* **39**, 447–468.
- FAISST, H. & ECKHARDT, B. 2004 Sensitive dependence on initial conditions in transition to turbulence in pipe flow. *J. Fluid Mech.* **504**, 343–352.
- FARANO, M., CHERUBINI, S., ROBINET, J.C. & DE PALMA, P. 2015 Hairpin-like optimal perturbations in plane Poiseuille flow. *J. Fluid Mech.* 775, R2.
- FARRELL, B.F. 1988 Optimal excitation of perturbations in viscous shear flow. Phys. Fluids 31, 2093.
- FORAME, P.C., HANSEN, R.J. & LITTLE, R.C. 1972 Observations of early turbulence in the pipe flow of drag reducing polymer solutions. *AIChE* 18, 213–217.
- GARG, P., CHAUDHARY, I., KHALID, M., SHANKAR, V. & SUBRAMANIAN, G. 2018 Viscoelastic pipe flow is linearly unstable. *Phys. Rev. Lett.* **121**, 024502.
- GIBSON, J.F. 2012 Channelflow: a spectral Navier–Stokes simulator in C++. *Tech. Rep.* University of New Hampshire.
- GRAHAM, M.D. 2014 Drag reduction and the dynamics of turbulence in simple and complex fluids. *Phys. Fluids* 26, 101301.
- HANSEN, R.J., LITTLE, R.C. & FORAME, P.G. 1973 Experimental and theoretical studies of early turbulence. *J. Chem. Engng Japan* 6, 310–314.
- HODA, N., JOVANOVIĆ, M.R. & KUMAR, S. 2008 Energy amplification in channel flows of viscoelastic fluids. J. Fluid Mech. 601, 407–424.
- HOF, B., JUEL, A. & MULLIN, T. 2003 Scaling of the turbulence transition threshold in a pipe. *Phys. Rev. Lett.* **91**, 244502.
- HOUSIADAS, K.D., BERIS, A.N. & HANDLER, R.A. 2005 Viscoelastic effects on higher order statistics and on coherent structures in turbulent channel flow. *Phys. Fluids* 17 (3), 035106.
- ITANO, T. & TOH, S. 2001 The dynamics of bursting process in wall turbulence. J. Phys. Soc. Japan 70, 703–716.
- JEONG, J. & FAZLE, H. 1995 On the identification of a vortex. J. Fluid Mech. 285, 69-94.
- JIMENEZ, J. & MOIN, P. 1991 The minimal flow unit in near-wall turbulence. J. Fluid Mech. 225, 213-240.
- KAWAHARA, G. 2005 Laminarization of minimal plane Couette flow: going beyond the basin of attraction of turbulence. *Phys. Fluids* **17** (4), 041702.
- KEEFE, L., MOIN, P. & KIM, J. 1992 The dimension of attractors underlying periodic turbulent Poiseuille flow. J. Fluid Mech. 242, 1–29.
- KERSWELL, R.R. 2005 Recent progress in understanding the transition to turbulence in a pipe. *Nonlinearity* **18**, R17–R44.
- KERSWELL, R.R. 2018 Nonlinear nonmodal stability theory. Annu. Rev. Fluid Mech. 50, 319–345.
- KIM, K., LI, C.F., SURESHKUMAR, R., BALACHANDAR, S. & ADRIAN, R.J. 2007 Effects of polymer stresses on eddy structures in drag-reduced turbulent channel flow. *J. Fluid Mech.* **584**, 281–299.
- KREISS, G., LUNDBLADH, A. & HENNINGSON, D.S. 1994 Bounds for threshold amplitudes in subcritical shear flows. *J. Fluid Mech.* 270, 175–198.
- LANDAHL, M.T. 1980 A note on an algebraic instability of inviscid parallel shear flows. *J. Fluid Mech.* **98**, 243–251.

- LEE, S.J. & ZAKI, T.A. 2017 Simulations of natural transition in viscoelastic channel flow. J. Fluid Mech. 820, 232–262.
- LEMOULT, G., AIDER, J.L. & WESFREID, J.E. 2012 Experimental scaling law for the subcritical transition to turbulence in plane Poiseuille flow. *Phys. Rev.* E **85**, 025303.
- LI, C.F., SURESHKUMAR, R. & KHOMAMI, B. 2006 Influence of rheological parameters on polymer induced turbulent drag reduction. J. Non-Newtonian Fluid Mech. 140, 23–40.
- LI, C.F., SURESHKUMAR, R. & KHOMAMI, B. 2015 Simple framework for understanding the universality of the maximum drag reduction asymptote in turbulent flow of polymer solutions. *Phys. Rev.* E **92**, 043014.
- LOPEZ, J.M., CHOUEIRI, G.H. & HOF, B. 2019 Dynamics of viscoelastic pipe flow at low Reynolds numbers in the maximum drag reduction limit. *J. Fluid Mech.* **874**, 699–719.
- LUCHINI, P. & BOTTARO, A. 2014 Adjoint equations in stability analysis. *Annu. Rev. Fluid Mech.* 46, 493–517.
 LUNDBLADH, A., HENNINGSON, D.S. & REDDY, S.C. 1994 Threshold amplitudes for transition in channel flows. *Trans. Turbul. Combust.* 1, 309–318.
- MESEGUER, Á. 2003 Streak breakdown instability in pipe Poiseuille flow. *Phys. Fluids* 15, 1203–1213.
- MIN, T., YOO, J.Y., CHOI, H. & JOSEPH, D.D. 2003 Drag reduction by polymer additives in a turbulent channel flow. *J. Fluid Mech.* 486, 213–238.
- MONOKROUSOS, A., BOTTARO, A., BRANDT, L., VITA, A.D. & HENNINGSON, D.S. 2011 Nonequilibrium thermodynamics and the optimal path to turbulence in shear flows. *Phys. Rev. Lett.* **106**, 134502.
- MULLIN, T. 2011 Experimental studies of transition to turbulence in a pipe. *Annu. Rev. Fluid Mech.* **43**, 1–24. MULLIN, T. & PEIXINHO, J. 2006 Recent observations of the transition to turbulence in a pipe. In *IUTAM Symposium on Laminar-Turbulent Transition*, pp. 45–55. Springer.
- NIKITIN, N. 2018 Characteristics of the leading Lyapunov vector in a turbulent channel flow. *J. Fluid Mech.* **849**, 942–967.
- ORSZAG, S.A. 1971 Accurate solution of the Orr–Sommerfeld stability equation. *J. Fluid Mech.* 4, 689–703. ORSZAG, S.A. & KELLS, L.C. 1980 Transition to turbulence in plane Poiseuille and plane Couette flow. *J. Fluid Mech.* 96, 159–205.
- PAGE, J., DUBIEF, Y. & KERSWELL, R.R. 2020 Exact traveling wave solutions in viscoelastic channel flow. *Phys. Rev. Lett.* **125** (15), 154501.
- PARK, J.S., SHEKAR, A. & GRAHAM, M.D. 2018 Bursting and critical layer frequencies in minimal turbulent dynamics and connections to exact coherent states. *Phys. Rev.* F **3**, 014611.
- PEIXINHO, J. & MULLIN, T. 2006 Decay of turbulence in pipe flow. Phys. Rev. Lett. 96, 094501.
- PEIXINHO, J. & MULLIN, T. 2007 Finite-amplitude thresholds for transition in pipe flow. *J. Fluid Mech.* **582**, 169–178.
- PERSHIN, A., BEAUME, C., EAVES, T.S. & TOBIAS, S.M. 2022 Optimizing the control of transition to turbulence using a Bayesian method. *J. Fluid Mech.* **941**, A25.
- PEYRET, R. 2002 Spectral Methods for Incompressible Viscous Flow. Springer.
- PFENNIGER, W. 1961 Transition in the inlet length of tubes at high Reynolds numbers. In *Boundary Layer and Flow Control*, pp. 970–980. Pergamon.
- PHILIP, J., SVIZHER, A. & COHEN, J. 2007 Scaling law for a subcritical transition in plane Poiseuille flow. *Phys. Rev. Lett.* **98**, 154502.
- PRINGLE, C.C.T & KERSWELL, R.R. 2010 Using nonlinear transient growth to construct the minimal seed for shear flow turbulence. *Phys. Rev. Lett.* **105**, 154502.
- PTASINSKI, P.K., BOERSMA, B.J., NIEUWSTADT, F.T.M., HULSEN, M.A., VAN DEN BRULE, B.H.A.A. & HUNT, J.C.R. 2003 Turbulent channel flow near maximum drag reduction: simulations, experiments and mechanisms. *J. Fluid Mech.* **490**, 251–291.
- RAM, A. & TAMIR, A. 1964 Structural turbulence in polymer solutions. J. Appl. Polym. Sci. 8, 2751–2762.
- REDDY, S.C., SCHMID, P.J., BAGGETT, J.S. & HENNINGSON, D.S. 1998 On stability of streamwise streaks and transition thresholds in plane channel flows. *J. Fluid Mech.* **365**, 269–303.
- REYNOLDS, O. 1883a An experimental investigation of the circumstances which determine whether the motion of water shall be direct or sinuous and of the law of resistance in parallel channels. *Proc. R. Soc. Lond.* A 35, 84–89.
- REYNOLDS, O. 1883b An experimental investigation of the circumstances which determine whether the motion of water shall be direct or sinuous and of the law of resistance in parallel channels. *Phil. Trans. R. Soc. Lond.* A **174**, 935–982.
- ROGGE, A.J. & PARK, J.S. 2022 On the underlying drag-reduction mechanisms of flow-control strategies in a transitional channel flow: temporal approach. *Flow Turbul. Combust.* 108, 1001–1016.
- ROTTA, J. 1956 Experimenteller beitrag zur entstehung turbulenter strömung im rohr. *Ingenieur-Archiv* 24, 258–281.

A. Martinez Ibarra and J.S. Park

- RUBIN, Y., WYGNANSKI, I.J. & HARITONIDIS, J.H. 1979 Further observations on transition in a pipe. In *Proceedings of the IUTAM Symposium*, pp. 19–26. Springer.
- SAMANTA, D., DUBIEF, Y., HOLZNER, M., SCHÄFER, C., MOROZOV, A.N., WAGNER, C. & HOF, B. 2013 Elasto-inertial turbulence. *Proc. Natl Acad. Sci. USA* 110, 10557–10562.
- SCHMID, P.J. 2007 Nonmodal stability theory. Annu. Rev. Fluid Mech. 39, 129-162.
- SCHMID, P.J. & HENNINGSON, D.S. 1994 Optimal energy density growth in Hagen-Poiseuille flow. J. Fluid Mech. 277, 197–225.
- SCHMID, P.J. & HENNINGSON, D.S. 2001 Stability and Transition in Shear Flows. Springer.
- SCHNEIDER, T.M., ECKHARDT, B. & YORKE, J.A. 2007 Turbulence transition and the edge of chaos in pipe flow. *Phys. Rev. Lett.* **99** (3), 034502.
- SID, S., TERRAPON, V.E. & DUBIEF, Y. 2018 Two-dimensional dynamics of elasto-inertial turbulence and its role in polymer drag reduction. *Phys. Rev. Fluids* 3, 011301.
- SRINIVAS, S.S. & KUMARAN, V. 2017 Effect of viscoelasticity on the soft-wall transition and turbulence in a microchannel. J. Fluid Mech. 812, 1076–1118.
- STONE, P.A. & GRAHAM, M.D. 2003 Polymer dynamics in a model of the turbulent buffer layer. *Phys. Fluids* **15**, 1247–1256.
- Sun, G., Wan, D. & Zhang, M. 2021 Nonlinear evolutions of streaky structures in viscoelastic pipe flows. J. Non-Newtonian Fluid Mech. 295, 104622.
- SURESHKUMAR, R., BERIS, A.N. & HANDLER, R.A. 1997 Direct numerical simulation of the turbulent channel flow of a polymer solution. *Phys. Fluids* **9**, 743–755.
- TERRAPON, V.E., DUBIEF, Y. & SORIA, J. 2015 On the role of pressure in elasto-inertial turbulence. J. Turbul. 16, 26–43.
- Toms, B. 1948 Some observations on the flow of linear polymer solutions through straight tubes at large Reynolds numbers. *Proceedings of the 1st International Congress on Rheology, North-Holland, Amsterdam*, vol. 2, pp. 135–141.
- Trefethen, L.N., Trefethen, A.E., Reddy, S.C. & Driscoll, T.A. 1993 Hydrodynamic stability without eigenvalues. *Science* **261**, 578–584.
- WALEFFE, F. 1997 On a self-sustaining process in shear flows. Phys. Fluids 9 (4), 883–900.
- WALEFFE, F. & WANG, J. 2005 Transition threshold and the self-sustaining process. In *IUTAM Symposium on Laminar-Turbulent Transition and Finite Amplitude Solutions*, pp. 85–106. Springer.
- WANG, J., GIBSON, J. & WALEFFE, F. 2007 Lower branch coherent states in shear flows: transition and control. *Phys. Rev. Lett.* **98** (20), 204501.
- WANG, S.N., GRAHAM, M.D., HAHN, F.J. & XI, L. 2014 Time-series and extended Karhunen-Loève analysis of turbulent drag reduction in polymer solutions. *AIChE J.* **60**, 1460–1475.
- WANG, S.N., SHEKAR, A. & GRAHAM, M.D. 2017 Spatiotemporal dynamics of viscoelastic turbulence in transitional channel flow. *J. Non-Newtonian Fluid Mech.* **244**, 104–122.
- WEBBER, G.A., HANDLER, R.A. & SIROVICH, L. 1997 The Karhunen-Loève decomposition of minimal channel flow. *Phys. Fluids* **9**, 1054–1066.
- WHITE, C.M. & MUNGAL, M.G. 2008 Mechanics and prediction of turbulent drag reduction with polymer additives. Annu. Rev. Fluid Mech. 40, 235–256.
- WHITE, F. 2006 Viscous Fluid Flow, 3rd edn. McGraw Hill.
- WYGNANSKI, I.J. & CHAMPAGNE, F.H. 1973 On transition in a pipe. Part 1. The origin of puffs and slugs and the flow in a turbulent slug. *J. Fluid Mech.* **59**, 281–351.
- WYGNANSKI, I.J., SOKOLOV, M. & FRIEDMAN, D. 1975 On transition in a pipe. Part 2. The equilibrium puff. *J. Fluid Mech.* **69**, 283–304.
- XI, L. 2009 Nonlinear dynamics and instabilities of viscoelastic fluid flow. PhD thesis, University of Wisconsin-Madison.
- XI, L. 2019 Turbulent drag reduction by polymer additives: fundamentals and recent advances. *Phys. Fluids* **31**, 121302.
- XI, L. & GRAHAM, M.D. 2010 Turbulent drag reduction and multistage transitions in viscoelastic minimal flow units. *J. Fluid Mech.* **647**, 421–452.
- XI, L. & GRAHAM, M.D. 2012 Dynamics on the laminar-turbulent boundary and the origin of the maximum drag reduction asymptote. *Phys. Rev. Lett.* **108**, 433–472.
- ZAKIN, J.L., NI, C.C., HANSEN, R.J. & REISCHMAN, M.M. 1977 Laser Doppler velocimetry studies of early turbulence. *Phys. Fluids* **20**, S85–S88.
- ZHANG, M., LASHGARI, I., ZAKI, T.A. & BRANDT, L. 2013 Linear stability analysis of channel flow of viscoelastic Oldroyd-B and FENE-P fluids. *J. Fluid Mech.* **737**, 249–279.
- ZHU, L. & XI, L. 2020 Inertia-driven and elastoinertial viscoelastic turbulent channel flow simulated with a hybrid pseudo-spectral/finite-difference numerical scheme. *J. Non-Newtonian Fluid Mech.* **286**, 104410.